

## Results from NA57

A. Dainese<sup>a</sup> (for the NA57\* Collaboration)

<sup>a</sup>Dipartimento di Fisica “G. Galilei”, Università degli Studi di Padova, Padova, Italy

The NA57 experiment has measured the production of strange and multi-strange hadrons in heavy-ion collisions at the CERN SPS. After briefly introducing the NA57 apparatus and analysis procedures, we present recent results on strangeness enhancement in Pb+Pb relative to p+Be collisions, on the study of the  $m_T$  distributions of strange particles, and on central-to-peripheral nuclear modification factors in Pb+Pb collisions at top SPS energy.

### 1. INTRODUCTION

The measurement of strangeness production in nucleus–nucleus collisions at high energy is a valuable tool to study the properties of the dense system expected to be formed in the collision.

The enhancement of the global production yield of strange and multi-strange baryons in nucleus–nucleus relative to proton-induced reactions was indicated, already at the beginning of the Eighties, as a signature for the phase transition from a hadron gas to a deconfined state of quarks and gluons (the quark-gluon plasma) [1]. Enhancements increasing with the strangeness content of the particle were first observed by WA97 at 158  $A$  GeV/ $c$  beam momentum [2]. The NA57 results, that we will present in Section 3, extend those of WA97 to a wider centrality range and to lower beam momentum of 40  $A$  GeV/ $c$ .

The transverse mass,  $m_T = \sqrt{m^2 + p_T^2}$ , and rapidity distributions of particles produced in nucleus–nucleus collisions are expected to be sensitive to the transverse and longitudinal expansion dynamics of the system formed in the collision [3]. Information on these dynamical effects can be extracted from the analysis of the shapes of the bulk kinematic distributions of strange particles (Section 4).

At large transverse momenta (for SPS energy) of 2–4 GeV/ $c$  the comparison of the binary-scaled  $p_T$ -differential yields of strange particles in central and in peripheral collisions may provide information on the mechanisms at play in the in-medium propagation and hadronization of energetic strange quarks (Section 5).

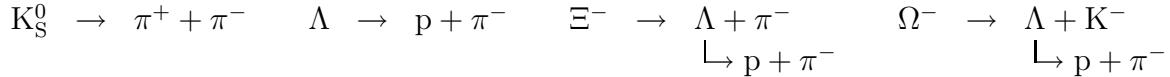
### 2. EXPERIMENTAL SETUP AND DATA ANALYSIS

The NA57 apparatus [4] was designed to study the production of strange and multi-strange hadrons in fixed-target heavy-ion collisions by reconstructing their weak decays

---

\*For the full list of NA57 authors and acknowledgements, see appendix ‘Collaborations’ of this volume.

into final states containing charged particles only:



(and charge-conjugates, for the hyperons). Tracks are reconstructed in the  $5 \times 5 \times 30$  cm<sup>3</sup> silicon pixel detector telescope which is placed 60 cm downstream of the target. Its acceptance covers about half a unit in rapidity at mid-rapidity and transverse momentum larger than about 0.5 GeV/ $c$ . The centrality trigger, based on charged multiplicity, was set so as to select approximately the most central 60% of the inelastic collisions.

The strange particles selection procedure is described in detail in [2,5]. The main decay-vertex identification criteria are the following: (a) the two decay trajectories are compatible with the hypothesis of having a common origin point; (b) the reconstructed decay vertex is well separated from the target. NA57 does not have charged-particle identification, but ambiguities among  $K_S^0$ ,  $\Lambda$  and  $\bar{\Lambda}$  are completely eliminated by means of kinematic cuts [2]. The high track-parameters resolution provided by the silicon pixel detectors allows to obtain final signal samples that are essentially background-free [5],[6]. Negatively charged particles,  $h^-$ , for the analysis presented in Section 5 are selected requiring that they point back to the interaction vertex, with a residual contamination of secondary tracks estimated to be smaller than 2%. For the measurement of the production yields and of the kinematic distributions (Sections 3 and 4) we corrected for acceptance and efficiency by assigning to every selected particle a weight, calculated on the basis of a Monte Carlo simulation [5].

The collision centrality is determined using the charged particle multiplicity  $N_{\text{ch}}$  in the pseudorapidity range  $2 < \eta < 4$ , sampled by the microstrip silicon detectors (MSD) as described in [7,8]. We fit the  $N_{\text{ch}}$ -differential Pb+Pb cross section  $d\sigma/dN_{\text{ch}}$ , as selected by the centrality trigger, assuming  $N_{\text{ch}} = q \cdot N_{\text{part}}^\alpha$  (a modified Wounded Nucleon model) [7], where  $N_{\text{part}}$  is the number of participants, i.e. nucleons participating in the primary nucleon–nucleon collisions, estimated from the Glauber model. The sample of collected events is subdivided in centrality classes, with  $N_{\text{ch}}$  limits corresponding to given fractions of the Pb+Pb inelastic cross section. For each class the average number of participants,  $\langle N_{\text{part}} \rangle$ , and of binary collisions,  $\langle N_{\text{coll}} \rangle$  are calculated, after the fit, from the Glauber model. For p+Be and p+Pb collisions, the values of  $\langle N_{\text{part}} \rangle$  are calculated directly from the Glauber model.

### 3. ENHANCEMENT: HOW IS STRANGENESS COOKED IN THE SYSTEM?

For each particle species, the corrected double-differential distribution is fitted to the expression:

$$d^2N/dm_T dy = f(y) m_T \exp(-m_T/T_{\text{app}}) , \quad (1)$$

where, within our acceptance of about a unit in rapidity around mid-rapidity  $y_{\text{cm}}$ , the shape of the rapidity distribution  $f(y)$  is taken to be gaussian for  $K_S^0$  and  $\bar{\Lambda}$ , and flat for the other strange particles [9]. The yield  $Y$  is calculated by integrating the fit expression over the phase-space region  $\{0 < p_T < \infty\} \times \{y_{\text{cm}} - 0.5 < y < y_{\text{cm}} + 0.5\}$ . The enhancement  $E$

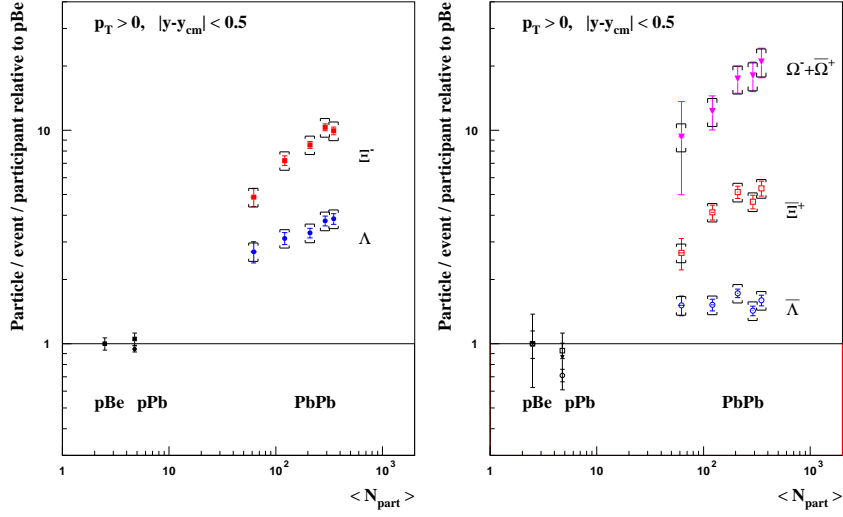


Figure 1. Centrality dependence of hyperon enhancements at 158  $A$  GeV/ $c$ . The bars indicate the statistical errors, while the bracket symbols represent the systematic errors.

is then defined as the yield per participant in a given centrality class in Pb+Pb divided by the yield per participant in p+Be:

$$E = (Y / \langle N_{\text{part}} \rangle)_{\text{Pb+Pb}} / (Y / \langle N_{\text{part}} \rangle)_{\text{p+Be}} \quad (2)$$

For the strangeness enhancement analysis we considered five centrality classes corresponding to the following intervals in percentiles of the Pb+Pb inelastic cross section, from the most central to the most peripheral: 0–4.5%, 4.5–11%, 11–23%, 23–40%, 40–53%. The enhancements in p+Pb relative to p+Be collisions are computed as well.

In Fig. 1 the hyperon enhancements at 158  $A$  GeV/ $c$  are shown as a function of  $\langle N_{\text{part}} \rangle$ . No enhancement in the yield per participant is observed when going from p+Be to p+Pb while a clear pattern of increasing enhancement with increasing strangeness content is observed in Pb+Pb, up to an enhancement of a factor about 20 for the triply-strange  $\Omega$  in the most central collisions. We note that the enhancements increase with centrality for all hyperons, except  $\bar{\Lambda}$ , which is even suppressed in p+Pb relative to p+Be.

The pattern  $E(\Lambda) < E(\Xi) < E(\Omega)$  is in agreement with the ‘historic’ predictions for a QGP scenario [1], the rationale behind these predictions being that the  $s$  and  $\bar{s}$  quarks, abundantly produced in the deconfined phase would recombine to form strange and multi-strange particles in a time much shorter than that required to produce them by successive rescattering interactions in a hadronic gas.

We illustrate the energy-dependence of the enhancements by showing the ratio of the enhancements at 40  $A$  GeV/ $c$  to those at 158  $A$  GeV/ $c$ , in Fig. 2, for  $\Lambda$ ,  $\bar{\Lambda}$  and  $\Xi^-$  (due to the limited statistics in p+Be collisions, the 40  $A$  GeV/ $c$  enhancements could not be calculated for rarer particles,  $\Xi^+$  and  $\Omega$ ). The enhancement is similar at the two energies, although its increase with centrality is steeper at 40  $A$  GeV/ $c$ , where we have indications, for the  $\Xi^-$  in particular, for a larger enhancement than at 158  $A$  GeV/ $c$  in the two most central classes. This experimental observation is in agreement with the prediction of a

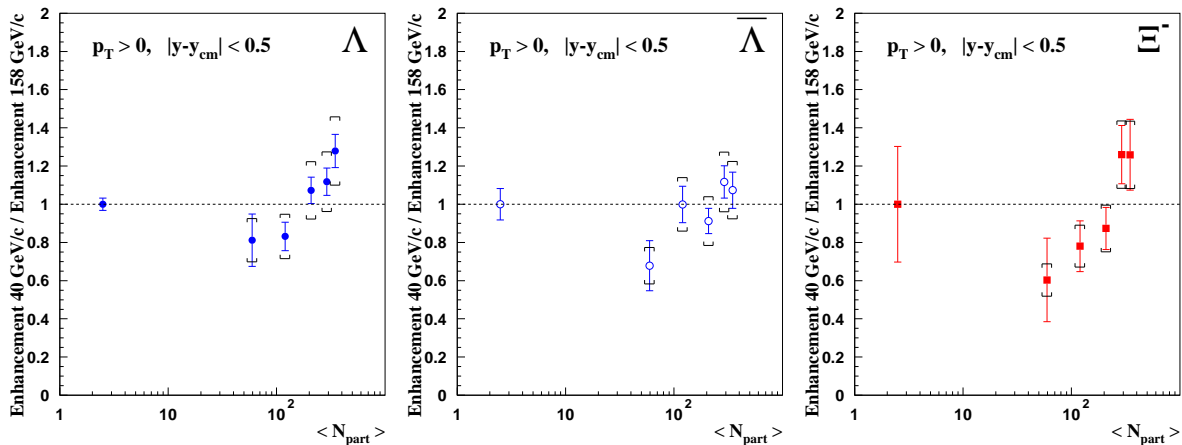


Figure 2. Ratios of the enhancements at 40  $A$  GeV/ $c$  to those at 158  $A$  GeV/ $c$ , as a function of centrality, for  $\Lambda$ ,  $\bar{\Lambda}$ , and  $\Xi^-$  (error symbols as in Fig. 1).

theoretical model [10], where the strangeness enhancement is obtained as a consequence of the removal of canonical suppression, when going from p-A to Pb+Pb collisions (see, *e.g.* [11] for a discussion). Note, however, that the model [10] does not reproduce correctly the centrality dependence nor the absolute magnitude of the enhancements.

#### 4. $m_T$ AND $y$ SPECTRA: HOW DOES THE SYSTEM EXPANSION AFFECT STRANGE PARTICLES?

The bulk of the kinematical distributions for particles produced in nucleus-nucleus interactions is expected to be shaped by the superposition of two effects: the thermal motion of the particles in the *fireball* and a pressure-driven radial (for  $m_T$ ) or longitudinal (for  $y$ ) collective flow, induced by the fireball expansion. Studies of the  $m_T$  spectra for  $\Lambda$ ,  $\Xi$ ,  $\Omega$  hyperons, and  $K_S^0$ , measured by NA57 in Pb+Pb collisions at 158 and 40  $A$  GeV/ $c$  were presented in [5] and [12], respectively. A study of the rapidity distributions in the NA57 acceptance,  $|y - y_{cm}| < 0.5$ , at 158  $A$  GeV/ $c$  was presented in [9].

The  $m_T$  spectra were analyzed in the framework of the *blast-wave* model [3]. The model assumes cylindrical symmetry for an expanding fireball in local thermal equilibrium and predicts the shape of the double-differential yield  $d^2N/dm_T dy$  for the different particle species, in terms of the kinetic freeze-out temperature  $T$  and of the radial velocity profile  $\beta_\perp(r)$ , that we parametrized as  $\beta_\perp(r) = \beta_S \cdot r/R_G$ , being  $\beta_S$  the flow velocity at the surface and  $R_G$  the outer radius. The fit to the experimental spectra allows to extract  $T$  and the average transverse flow velocity  $\langle \beta_\perp \rangle = 2/3 \cdot \beta_S$  [5]. The results of the simultaneous fits to all particle species, centrality-integrated over the range 0–53% covered by NA57, are shown in Fig. 3 for collisions at 40 (left) and 158  $A$  GeV/ $c$  (centre). The resulting kinetic freeze-out temperature and average transverse flow velocity values are:

$$T = (118 \pm 5 \pm 11) \text{ MeV}, \quad \langle \beta_\perp \rangle = 0.38 \pm 0.01 \pm 0.01 \quad \text{at } 40 \text{ } A \text{ GeV}/c$$

$$T = (144 \pm 7 \pm 14) \text{ MeV}, \quad \langle \beta_\perp \rangle = 0.40 \pm 0.01 \pm 0.01 \quad \text{at } 158 \text{ } A \text{ GeV}/c$$

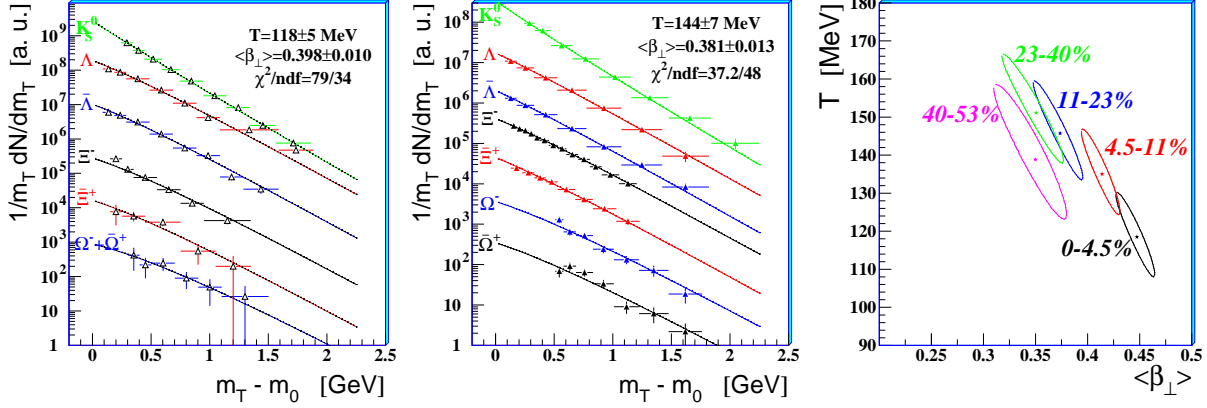


Figure 3. Blast-wave fits to the transverse mass spectra of strange particles for the 53% most central Pb+Pb collisions at 158 (left) and at 40 (middle)  $A$  GeV/ $c$ . Right: centrality dependence of  $T$  and  $\langle\beta_{\perp}\rangle$  at 158  $A$  GeV/ $c$  ( $1\sigma$  contour plots) [5,12].

where the first error is statistical and the second is systematic. A lower thermal freeze-out temperature is measured at lower collision energy, while the transverse flow velocities are found to be compatible within errors. When performed separately in the five centrality classes at 158  $A$  GeV/ $c$ , the analysis shows an increase of  $T$  and a decrease of  $\langle\beta_{\perp}\rangle$  from central (0–4.5%) to semi-peripheral (40–53%) collisions, as presented in the Fig. 3 (right). This may be interpreted as an indication for earlier freeze-out of the system at lower energy.

In order to extract information about the longitudinal expansion dynamics from the rapidity distributions, we used the blast-wave model [3], with a Bjorken-expansion scenario [13] folded with a thermal distribution of the fluid elements (see [9] for details of the analysis). Since, within the limited rapidity acceptance of the NA57 telescope ( $|y - y_{\text{cm}}| < 0.5$ ), the sensitivity is not sufficient to constrain both the kinetic freeze-out temperature and the longitudinal flow velocity, we fixed the temperature to the value of about 144 MeV extracted from the  $m_T$  analysis, and we fitted only the longitudinal flow velocity. The distributions of all strange particles under study can be fitted simultaneously ( $\chi^2/\text{ndf} \approx 1$ ) [9]. The resulting average longitudinal flow velocity is  $\langle\beta_L\rangle = 0.42 \pm 0.03(\text{stat})$ , similar to  $\langle\beta_{\perp}\rangle$  (see above), suggesting large nuclear stopping along the beam direction.

## 5. $R_{\text{CP}}$ : HOW DOES THE MEDIUM AFFECT $s$ -QUARK PROPAGATION AND HADRONIZATION?

At RHIC energies, the central-to-peripheral nuclear modification factor

$$R_{\text{CP}}(p_T) = \frac{\langle N_{\text{coll}} \rangle_{\text{P}}}{\langle N_{\text{coll}} \rangle_{\text{C}}} \times \frac{d^2 N_{\text{AA}}^{\text{C}}/dp_T dy}{d^2 N_{\text{AA}}^{\text{P}}/dp_T dy} \quad (3)$$

has proven to be a powerful tool for the study of parton propagation in the dense system formed in nucleus–nucleus collisions (see, *e.g.* [14]). At high  $p_T$  ( $\gtrsim 7$  GeV/ $c$ ),  $R_{\text{CP}}$  is found to be suppressed by a factor 3–4 with respect to unity (at  $\sqrt{s_{\text{NN}}} = 200$  GeV), for all particle species; this is interpreted as a consequence of parton energy loss in the medium, prior to fragmentation *outside* the medium. At intermediate transverse momenta (2–5 GeV/ $c$ ), instead, partons are believed to lose energy *and* hadronize *inside* the medium via the mechanism of recombination; this would originate the measured pattern of smaller suppression for baryons relative to mesons.

The study of  $R_{\text{CP}}$  and of its particle-species dependence at top SPS energy allows to test for these phenomena at an energy smaller by about one order of magnitude ( $\sqrt{s_{\text{NN}}} = 17.3$  GeV). While measurements of the  $\pi^0$   $R_{\text{CP}}$  by the WA98 Collaboration, supporting the presence of parton energy loss effects, were published already in 2002 [15], the first data on the particle-species dependence have been presented by the NA57 Collaboration in [6] and by the NA49 Collaboration at this Quark Matter 2005 conference [16].

In order to exploit the full sample of collected data, we calculate  $R_{\text{CP}}(p_T)$  for  $h^-$ ,  $K_S^0$ ,  $\Lambda$  and  $\bar{\Lambda}$  using  $p_T$  distributions which are not corrected for geometrical acceptance and reconstruction/selection efficiency. We have verified [6] on a subsample of events that the corrections do not depend on the event centrality over the full transverse momentum range covered,  $0.5 < p_T \lesssim 4$  GeV/ $c$ . Figure 4 (left) shows the results for the 0–5%/40–55%  $R_{\text{CP}}$ . The results are in qualitative agreement with those presented by NA49 [16] for charged pions, charged kaons and protons plus antiprotons (a quantitative comparison of NA57  $K_S^0$  and NA49  $K^\pm$  is at the moment not straightforward, since different definitions of the reference peripheral class are used by the two experiments).

In the right-hand panel of Fig. 4 we compare our  $K_S^0$  data to predictions provided by X.-N. Wang, obtained from a perturbative QCD-based calculation [17], including (thick line) or excluding (thin line) in-medium parton energy loss. The initial gluonic rapidity density of the medium,  $dN_g/dy$ , was scaled down from that needed to describe RHIC data, according to the decrease by about a factor 2 in  $dN_{\text{ch}}/dy$  from 200 to 17.3 GeV c.m.s. energy. The curve without energy loss shows a large ‘Cronin-enhancement’ toward high  $p_T$ , included in the calculation via an initial-state partonic intrinsic transverse momentum broadening, tuned on the original Cronin effect data [18]. This enhancement is not present in our  $K_S^0$  data, that are better described by the curve including energy loss. As a cross-check, we compared the  $R_{\text{CP}}$  value predicted by X.-N. Wang with energy loss to the prediction of an independent model of parton energy loss, the Parton Quenching Model (PQM), that describes several energy-loss-related observables at RHIC energies [19]. The two models predict a similar energy loss effect at SPS energy, i.e. a reduction of the 0–5%/40–55%  $R_{\text{CP}}$  (for  $p_T \gtrsim 4$  GeV/ $c$ ) by about a factor 2, with respect to the value calculated without energy loss.

Figure 5 shows the comparison for  $K_S^0$  and  $\Lambda$  at SPS and RHIC (STAR data for Au+Au at  $\sqrt{s_{\text{NN}}} = 62.4$  GeV (preliminary) [20] and 200 GeV [14]). In the  $p_T$  range covered by our data, up to 4 GeV/ $c$ , the relative pattern for  $K_S^0$  and  $\Lambda$  is similar at the three energies, while absolute values decrease gradually with increasing energy, from top SPS to top RHIC energy. The similarity of the  $\Lambda$ – $K$  pattern to that observed at RHIC may be taken as an indication for recombination effects at SPS energy. This interpretation is also reminiscent of the ‘historic’ argument for the strangeness enhancement in a QGP scenario,

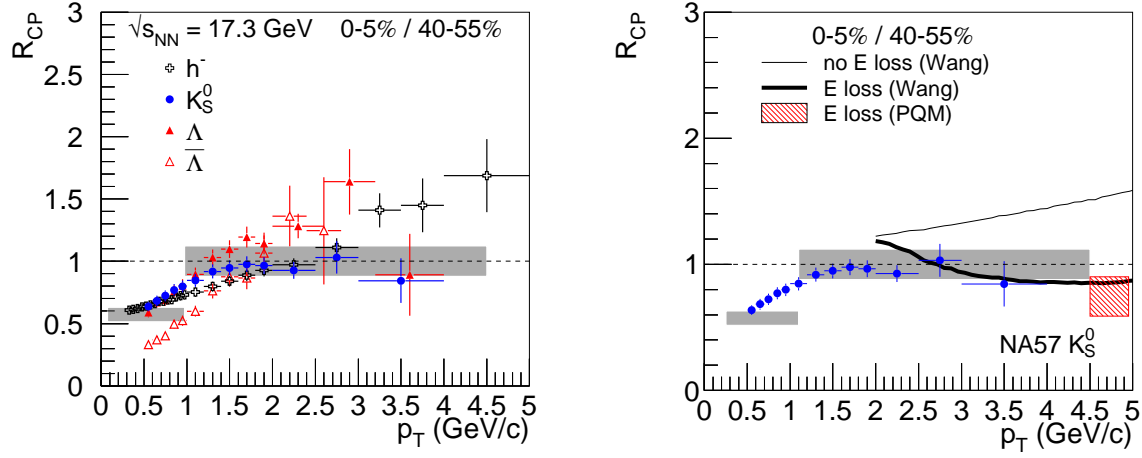


Figure 4. Left:  $R_{CP}(p_T)$  for  $h^-$ ,  $K_S^0$ ,  $\Lambda$  and  $\bar{\Lambda}$  in Pb-Pb collisions at  $\sqrt{s_{NN}} = 17.3$  GeV [6]; bars are the sum of statistical and point-by-point systematic errors; shaded bands centered at  $R_{CP} = 1$  represent the systematic error due to the uncertainty in the ratio of the values of  $\langle N_{coll} \rangle$  in each class; shaded bands at low  $p_T$  represent the values expected for scaling with the number of participants, with their systematic error. Right: the  $K_S^0$   $R_{CP}(p_T)$  compared to predictions [17,19] with and without energy loss.

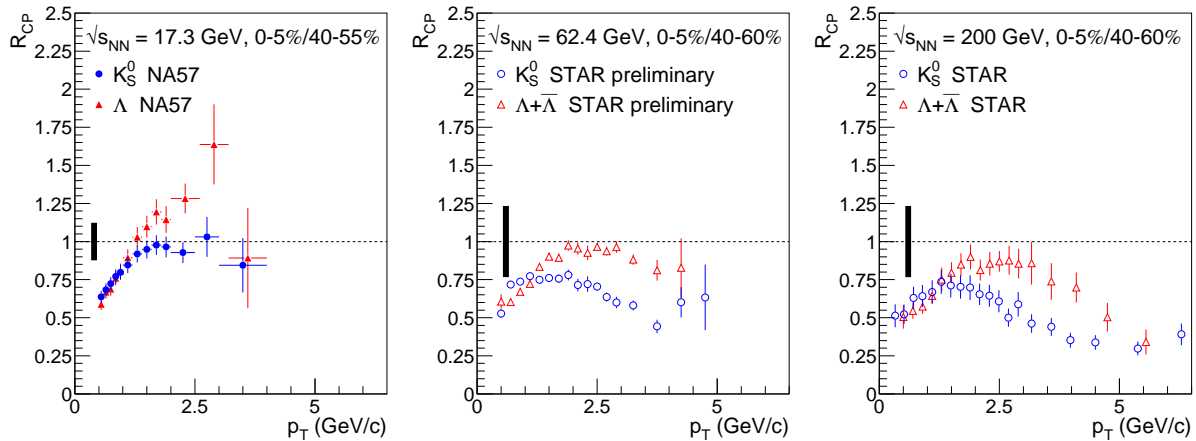


Figure 5.  $R_{CP}(p_T)$  for  $K_S^0$  and  $\Lambda$  at  $\sqrt{s_{NN}} = 17.3$  GeV [6] from NA57, and at  $\sqrt{s_{NN}} = 62.4$  GeV [20] and 200 GeV/c [14] from STAR ( $\Lambda + \bar{\Lambda}$ ).

where strange and non-strange quarks would *recombine* with other quarks in the system to form strange and multi-strange hyperons. We note, however, that the  $\Lambda$ -K pattern may also be understood in terms of larger Cronin effect for  $\Lambda$  with respect to K.

## 6. CONCLUSIONS

In summary, the NA57 experiment has measured:

- A hierarchical pattern according to strangeness content for hyperon enhancements ( $p_T$ -integrated yield per participant in Pb+Pb relative to p+Be):  $E(\Lambda) < E(\Xi) < E(\Omega)$  at 158 A GeV/c and  $E(\Lambda) < E(\Xi)$  at 40 A GeV/c. This pattern was predicted as a consequence of a phase transition to a deconfined quark-gluon plasma [1].
- Strange particles  $m_T$  and rapidity distributions that can be described within a hydrodynamical picture, with a superposition of thermal motion with a kinetic freeze-out temperature  $T \simeq 144$  MeV and collective flow with similar transverse and longitudinal average velocities  $\langle\beta_\perp\rangle \simeq \langle\beta_L\rangle \simeq 0.4$ , in the centrality range 0–53% at top SPS energy.
- A central-to-peripheral  $R_{CP}$  pattern qualitatively similar to that observed at RHIC, although higher in the absolute values. In particular, the difference between  $K_S^0$  and  $\Lambda$  suggests a recombination-induced baryon/meson effect also at SPS energy, and the comparison of the  $K_S^0$  data with theoretical calculations favours the presence of parton energy loss. This issue could be clarified with a systematic analysis of the p+Pb/p+Be and Pb+Pb/p+Be nuclear modification factors, that would allow to disentangle Cronin enhancement and energy loss suppression.

## REFERENCES

1. J. Rafelski and B. Müller, Phys. Rev. Lett. 48 (1982) 1066; ibidem 56 (1986) 2334.
2. E. Andersen *et al.*, WA97 Coll., Phys. Lett. B 433 (1998) 209; R.A. Fini *et al.*, WA97 Coll., J. Phys. G 27 (2001) 375.
3. E. Schnedermann *et al.*, Phys. Rev. C 48 (1993) 2462; ibidem 50 (1994) 1675.
4. V. Manzari *et al.*, NA57 Coll., J. Phys. G 25 (1999) 473.
5. F. Antinori *et al.*, NA57 Coll., J. Phys. G 30 (2004) 823.
6. F. Antinori *et al.*, NA57 Coll., Phys. Lett. B 623 (2005) 15.
7. F. Antinori *et al.*, NA57 Coll., Eur. Phys. J. C 18 (2000) 57.
8. F. Antinori *et al.*, NA57 Coll., J. Phys. G 31 (2005) 321.
9. F. Antinori *et al.*, NA57 Coll., J. Phys. G *in print*, arXiv:nucl-ex/0509009.
10. A. Tounsi *et al.*, Nucl. Phys. A 715 (2003) 565c.
11. F. Antinori, J. Phys. G 30 (2004) S725.
12. G.E. Bruno, for the NA57 Coll., J. Phys. G 31 (2005) S127.
13. J.D. Bjorken, Phys. Rev. D 27 (1983) 140.
14. J. Adams *et al.*, STAR Coll., Phys. Rev. Lett. 92 (2004) 052302.
15. M.M. Aggarwal *et al.*, WA98 Coll., Eur. Phys. J. C 23 (2002) 225.
16. C. Höhne, A. László, for the NA49 Coll., *these proceedings*.
17. X.-N. Wang, Phys. Rev. C 61 (2000) 064910; Phys. Rev. Lett. 81 (1998) 2655; Phys. Lett. B 595 (2004) 165; private communication.
18. J. Cronin *et al.*, Phys. Rev. D 11 (1975) 3105; D. Antreasyan *et al.*, Phys. Rev. D 19 (1979) 764.
19. A. Dainese *et al.*, Eur. Phys. J. C 38 (2005) 461; private communication.
20. S. Salur, for the STAR Coll., *these proceedings*.